ISBN: 978-3-95450-214-1 ISSN: 2673-5490 doi:10.18429/JACoW-IPAC2021-WEPAB318

PREDICTION AND CLUSTERING OF LONGITUDINAL PHASE SPACE IMAGES AND MACHINE PARAMETERS USING NEURAL NETWORKS AND K-MEANS ALGORITHM

M. Maheshwari, D. J. Dunning*, J. K. Jones, M. P. King, H. R. Kockelbergh, A. E. Pollard
ASTeC, Cockcroft Institute, STFC Daresbury Laboratory, UK

Abstract

Machine learning algorithms were used for image and parameter recognition and generation with the aim to optimise the CLARA facility at Daresbury, using start-to-end simulation data. Convolutional and fully connected neural networks were trained using TensorFlow-Keras for different instances, with examples including predicting Longitudinal Phase Space (LPS) images with machine parameters as input and FEL parameter prediction (e.g. pulse energy) from LPS images. The K-means clustering algorithm was used to cluster the LPS images to highlight patterns within the data. Machine learning techniques can enhance the way large amounts of data are processed and analysed and so have great potential for application in accelerator science R&D.

INTRODUCTION

CLARA is an existing test facility at Daresbury Laboratory; the operational parts can achieve 50 MeV/c electron beam momentum with the full machine capable of reaching 250 MeV/c. A full energy beam extraction line (FEBE) with a user station is currently being installed [1]. Shown in Fig. 1 is a possible upgrade to CLARA using high-gradient X-band RF technology to reach a maximum beam momentum of 1 GeV/c, known as XARA (X-band Accelerator for Research and Applications) [2]. This would allow for novel undulator light production, attosecond pulse generation, and the enhancement of current accelerator science via increased beam momentum and X-band development. Machine learning algorithms applied to CLARA/XARA would enhance its capability for R&D by providing rapid access to slow or invasive measurements through virtual diagnostics, and through more comprehensively exploring its parameter space and rapidly optimising to desired operating conditions.

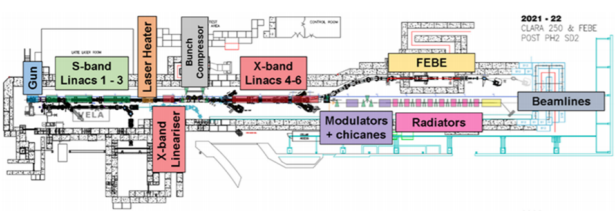

Figure 1: Schematic layout of CLARA with potential upgrade XARA overlaid [2]. The total length is roughly 90 m.

In this paper, two machine learning techniques were applied, with the first being a Neural Network (NN) used to recreate beam images and FEL parameters. NNs are computational systems designed to learn and translate data from one form to another. A neural network is made up of input and output neurons with weighted links in between; it learns to map inputs onto outputs by adjusting the weights between neurons using an optimisation algorithm. A convolutional neural network is a widely used extension to neural networks designed to process two-dimensional data.

An unsupervised clustering algorithm known as K-means was then used to cluster beam images as the second machine learning technique. Unsupervised algorithms are used to cluster un-labelled data according to defining features; the aim is to find patterns within the data. K-means is one such algorithm and works by creating k centroids, where k is the number of clusters chosen by the user. Then, the algorithm works to minimise the squared Euclidean distance between each data point and the nearest centroid to it [3].

METHOD

The data used in this study was ~10,000 start–to-end simulations of the accelerator and FEL, generated using the simulation code ASTRA (to the linac 1 exit), Elegant for the rest, and Genesis for the FEL data [4]. 17 machine parameters (e.g. linac RF phases and amplitudes) were varied up to the undulator; only parameters that have a particular effect on the Longitudinal Phase Space (LPS) were changed. Then, using the 6D bunch distributions produced, LPS images were created with two different choices regarding extents. The first, referred to as Region Of Interest (ROI) images, were created by calculating the maximum and minimum values of the z-positions and beam energies for each individual distribution and binning the particles in a 2D histogram defined by these extents to create 100×100 pixel images. For the other set, the maxima and minima were taken over all distributions, for a fixed 'screen size' (hence referred to as non-ROI images): 200×200 pixels was chosen to give reasonable resolution and computational speed. For simplicity this study used only images, so some information is lost for the ROI set but the extent data has also been used for studies beyond the scope of this paper.

For the first part of the study, the 200×200 pixel LPS images were used as input to a convolutional neural network (Fig. 2), with the corresponding FEL pulse energy and bandwidth values as output. This was implemented in Keras and it consisted of a (3×3) convolutional layer followed by a (2×2) max pooling layer, repeated 5 times, followed by

* david.dunning@stfc.ac.uk

ISBN: 978-3-95450-214-1 ISSN: 2673-5490 doi:10.18429/JACoW-IPAC2021-WEPAB318

4 dense layers (including the output layer). The first 3 convolutional layers had 8 filters, and the last 2 had 16 filters. The learning rate used was 4×10^{-5}. The model trained to stability within 70 epochs.

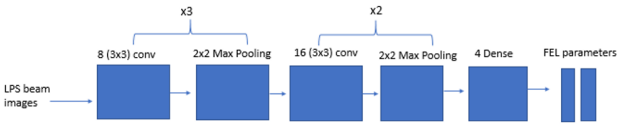

Figure 2: The neural network used to predict FEL pulse energy and bandwidth values from LPS beam images (200×200 pixels). There are 5 convolutional layers and 5 max pooling layers, followed by 4 dense layers.

Previous studies [5, 6] used NNs to predict LPS images from machine parameters; the same method was used here to predict both kinds of images (ROI and non-ROI) separately using the same neural network architecture but with different output neurons. This network (Fig. 3) was also implemented in Keras and consisted of 5 dense layers, with: 17, 100, 500, 1000 neurons respectively and 10k neurons in the output layer for the ROI images and 40k neurons for the non-ROI images. The learning rate used was 4×10^{-3}. The models trained to stability within 60 epochs. In all three cases: Adam was the optimiser, the batch size used was 100 and Early Stopping Rounds was used with 1000 epochs (set to minimise loss), dropout layers and learning rate reduction were used to help decrease over-fitting. The model architectures were decided after trial and error. The activation functions used for the hidden layers were leaky rectified linear units and mean squared error in the predictions was the cost function. Of the ~10,000 images, 8244 (90%) were used to train the model and 916 (10%) for validation.

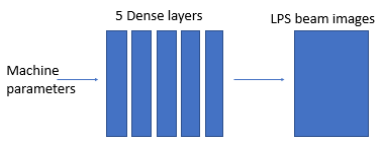

Figure 3: The neural network used to predict LPS beam images (ROI and non-ROI) from 17 machine parameters. There are 6 dense layers.

For the second part of the study, Principal Component Analysis (PCA) was first applied to both kinds of beam images with variance at 0.98. PCA is a method that decreases the dimension of the input data while preserving most of the important information, allowing the following algorithm to run faster. The images were then separated into 8 clusters using K-means (with a defined random state to ensure consistency in the clusters), to find out if there were any patterns within the image dataset and the corresponding parameters. The number of clusters used was established after using the elbow method. The method was also extended to 2D binning by both ROI and non-ROI cluster for further analysis.

RESULTS

Figure 4 shows how the predicted FEL parameters (FEL pulse energy and bandwidth) from the CNN compared to the actual values. Figures 5 and 6 show the mean absolute percentage error histograms of the FEL pulse energy and bandwidth predictions.

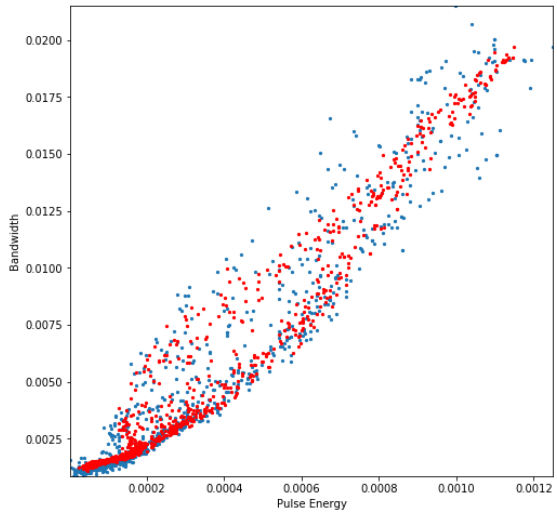

Figure 4: Scatter plot of predicted FEL pulse energy and relative pulse bandwidth (red) against real values (blue).

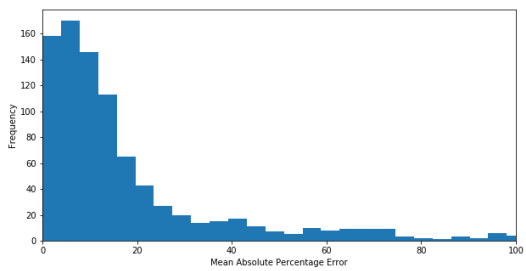

Figure 5: Mean absolute percentage error histogram of FEL pulse energy. The mean percentage error is 30%.

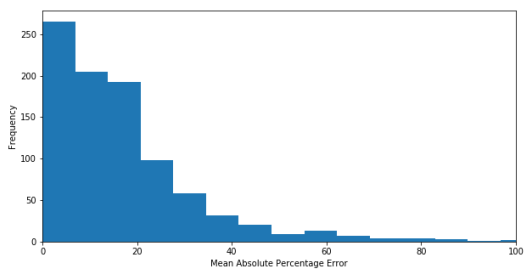

Figure 6: Mean absolute percentage error histogram of FEL bandwidth. The mean percentage error is 17.1%.

The FEL pulse energy vs. bandwidth scatter plot in Fig. 4 shows the predicted values (red) and the corresponding true values (blue) to be in good agreement as the general shape of the predicted spread of values overlap well with the actual values. The mean absolute percentage error histograms for pulse energy and bandwidth shown in Figs. 5 and 6 respectively, are positively skewed; this suggests accuracy in

ISBN: 978-3-95450-214-1 ISSN: 2673-5490 doi:10.18429/JACoW-IPAC2021-WEPAB318

the predictions. For the pulse energy histogram, 71.7% of test values have a percentage error of 20% or less and the mean percentage error is 30%; for the bandwidth histogram, 70.6% of test values have a percentage error of 20% or less with a mean percentage error of 17.1%. Neural network models will give slightly different results each time they are run although the percentages mentioned above varied only by a few units with the model used.

For the LPS image prediction, as shown in Fig. 7, the position of the predicted beam in the non-ROI beam image was picked up well by the model but with some error in its brightness and shape, in comparison to the actual image. The general shape of the predicted beam was well defined for the ROI beam image with variations in brightness identified by the model too. In general, the ROI beam image was predicted more accurately as the mean squared error was significantly lower than for the non-ROI case. This disparity may be because the non-ROI images contain more blank space and poorer resolution of the beam. Subsequent work beyond the scope of this paper therefore used ROI images in combination with scalar position/energy extents, as in [5, 6]. The 2D matrix of common beam images between clusters in Fig. 8 shows that the ROI beam images were clustered by the slope of the beam mainly and the non-ROI beam images were clustered depending on the width of the beam (beam duration) or its vertical position on the screen (beam energy). The ROI beam images were distributed evenly within these

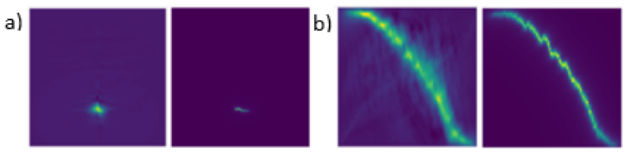

Figure 7: Example predicted and real LPS beam images (vertical/horizontal axes are energy/time). a) Left: Predicted non-ROI beam image. Right: real equivalent. b) Left: Predicted ROI beam image. Right: real equivalent.

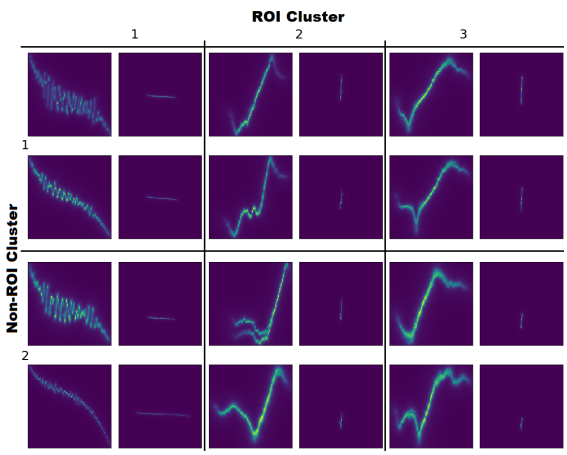

Figure 8: The labelled columns and rows represent the first 3 ROI clusters and 2 non-ROI clusters respectively, each with two example beam image pairs common to those clusters.

clusters but the model had trouble clustering the non-ROI images with smaller and less-defined shapes of the beam, so the non-ROI clusters were unevenly populated.

Examining the average machine parameters within each cluster showed a relationship between the parameters and the beam position/shape (not shown here). For the non-ROI beam images, the linac amplitudes corresponded to the energy level (vertical position in the image). For the ROI beam images, the linac phases correspond to the gradient of the beam. The relation of the individual clusters to FEL bandwidth is shown in Fig. 9. Clear regions of clusters can be seen suggesting that the clustering algorithm distinguished features relevant to FEL performance in the LPS images.

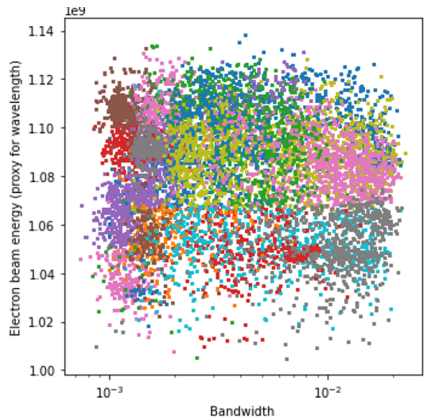

Figure 9: FEL bandwidth and electron beam energy (proxy for wavelength) for all simulations. Each colour corresponds to a different cluster of the 64 defined by the 2D ROI/non-ROI image clustering (some contain very few points).

CONCLUSION

The model predicted the majority of FEL parameters accurately with low error. The recreated beam images were also very representative; they captured the beam image pattern and brightness well (in the case of the ROI image) and the position of the beam was accurate for the non-ROI beam image. The patterns in the beam images were also well separated by the clustering algorithm. We plan to apply the neural network to the accelerator as a virtual diagnostic tool, allowing beam images and corresponding parameters to be available quickly and easily. The clustering algorithm could be used to create a collection of potential operating conditions for both users and operators to select from, which for each cluster relates FEL performance and beam images back to the required machine settings. The next step for this work will be to transfer these techniques from simulations to the real machine, where issues such as image artefacts and variable machine performance over time will be present. It is anticipated that further machine learning techniques such as artefact removal and transfer learning will be of use.

ISBN: 978-3-95450-214-1 ISSN: 2673-5490 doi:10.18429/JACoW-IPAC2021-WEPAB318

REFERENCES

[1] *D.* Angal-Kalinin *et al.*, "Design, specifications, and first beam measurements of the compact linear accelerator for research and applications front end", *Phys. Rev. Accel. Beams*, vol. 23, no. 4, Apr. 2020. doi:10.1103/PhysRevAccelBeams.23.044801

[2] D. J. Dunning, L. S. Cowie, and J. K. Jones, "XARA: X-Band Accelerator for Research and Applications", in *Proc. 39th Int. Free Electron Laser Conf. (FEL'19)*, Hamburg, Germany, Aug. 2019, pp. 715–718. doi:10.18429/JACoW-FEL2019-THP066

[3] *A.* Coates and A. Y. Ng, "Learning Feature Representations with K-means", in *Neural Networks: Tricks of the Trade. Lecture Notes in Computer Science*, G. Montavon, G. B. Orr, K. R. Müller, Eds. Berlin, Heidelberg, Germany: Springer, 2012, pp. 561–580.

[4] D. J. Dunning, H. M. Castañeda Cortés, J. K. Jones, and N. Thompson, "Multi-Objective FEL Design Optimisation Using Genetic Algorithms", in *Proc. 39th Int. Free Electron Laser Conf. (FEL'19)*, Hamburg, Germany, Aug. 2019, pp. 711–714. doi:10.18429/JACoW-FEL2019-THP065

[5] A. Edelen, N. Neveu, C. Emma, D. Ratner, and C. Mayes, "Machine Learning Models for Optimization and Control of X-ray Free Electron Lasers", in *Proc. Second Workshop on Machine Learning and the Physical Sciences (NeurIPS'19)*, Vancouver, Canada, Dec. 2019, paper 90, pp. 1-5.

[6] C. Emma, A. Edelen, M. J. Hogan, B. O'Shea, G. White, and V. Yakimenko, "Machine learning-based longitudinal phase space prediction of particle accelerators", *Phys. Rev. Accel. Beams*, vol. 21, no. 11, Nov. 2018. doi:10.1103/physrevaccelbeams.21.112802